A&A 582, L4 (2015)
DOI: 10.1051/0004-6361/201527254

Astronomy & Astrophysics

Letter to the Editor

Detection of extragalactic argonium, ArH^+, toward PKS 1830−211⋆

Holger S. P. Müller[1], Sébastien Muller[2], Peter Schilke[1], Edwin A. Bergin[3], John H. Black[2], Maryvonne Gerin[4], Dariusz C. Lis[5,6], David A. Neufeld[7], and Sümeyye Suri[1]

[1] I. Physikalisches Institut, Universität zu Köln, Zülpicher Str. 77, 50937 Köln, Germany
e-mail: hspm@ph1.uni-koeln.de
[2] Department of Earth and Space Sciences, Chalmers University of Technology, Onsala Space Observatory, 43992 Onsala, Sweden
[3] Department of Astronomy, The University of Michigan, 500 Church Street, Ann Arbor, MI 48109-1042, USA
[4] LERMA, Observatoire de Paris, PSL Research University, CNRS, Sorbonne Universités, UPMC Univ. Paris 06, École normale supérieure, 75005 Paris, France
[5] LERMA, Observatoire de Paris, PSL Research University, CNRS, Sorbonne Universités, UPMC Univ. Paris 06, 75014 Paris, France
[6] Cahill Center for Astronomy and Astrophysics 301-17, California Institute of Technology, Pasadena, CA 91125, USA
[7] Department of Physics and Astronomy, Johns Hopkins University, Baltimore, MD 21218, USA

Received 26 August 2015 / Accepted 22 September 2015

ABSTRACT

Context. Argonium has recently been detected as a ubiquitous molecule in our Galaxy. Model calculations indicate that its abundance peaks at molecular fractions in the range of 10^{-4} to 10^{-3} and that the observed column densities require high values of the cosmic ray ionization rate. Therefore, this molecular cation may serve as an excellent tracer of the very diffuse interstellar medium (ISM), as well as an indicator of the cosmic ray ionization rate.
Aims. We attempted to detect ArH^+ in extragalactic sources to evaluate its diagnostic power as a tracer of the almost purely atomic ISM in distant galaxies.
Methods. We obtained ALMA observations of a foreground galaxy at $z = 0.89$ in the direction of the lensed blazar PKS 1830−211.
Results. Two isotopologs of argonium, $^{36}ArH^+$ and $^{38}ArH^+$, were detected in absorption along two different lines of sight toward PKS 1830−211, known as the SW and NE images of the background blazar. The argonium absorption is clearly enhanced on the more diffuse line of sight (NE) compared to other molecular species. The isotopic ratio $^{36}Ar/^{38}Ar$ is 3.46 ± 0.16 toward the SW image, i.e., significantly lower than the solar value of 5.5.
Conclusions. Our results demonstrate the suitability of argonium as a tracer of the almost purely atomic, diffuse ISM in high-redshift sources. The evolution of the isotopic ratio with redshift may help to constrain nucleosynthetic scenarios in the early Universe.

Key words. quasars: absorption lines – galaxies: ISM – galaxies: abundances – nuclear reactions, nucleosynthesis, abundances – astrochemistry – quasars: individual: PKS 1830-211

1. Introduction

Our knowledge of interstellar hydride species has been considerably increased by recent submillimeter missions, in particular the Heterodyne Instrument for the Far-Infrared (HIFI) on board *Herschel* and the German REceiver At Terahertz frequencies (GREAT) on board the Stratospheric Observatory for Far-Infrared Astronomy (SOFIA), but also ground-based observatories, such as the Atacama Pathfinder EXperiment (APEX). The newly detected hydride species are SH^+ (Menten et al. 2011), OH^+ (Wyrowski et al. 2010), H_2O^+ (Ossenkopf et al. 2010), H_2Cl^+ (Lis et al. 2010), HCl^+ (De Luca et al. 2012), SH (Neufeld et al. 2012), and, most recently, ArH^+ (Barlow et al. 2013; Schilke et al. 2014). OH^+ and H_2O^+ were also observed extensively in extragalactic sources (van der Werf et al. 2010; Weiß et al. 2010; González-Alfonso et al. 2013).

The large column densities of OH^+ with respect to H_2O^+ were explained by both molecules residing preferentially in the largely atomic, diffuse interstellar medium (ISM), with the largest fractional abundances at a molecular fraction of around 0.04, and their unexpectedly large column densities require cosmic ray ionization rates ζ considerably larger than in the dense ISM (Hollenbach et al. 2012; Indriolo et al. 2015).

The ArH^+ cation was initially identified toward the Crab Nebula through its $J = 1{-}0$ and $2{-}1$ transitions, with OH^+ $1{-}0$ as the only other emission feature in the spectrum recorded with the Spectral and Photometric Image REceiver (SPIRE) on board *Herschel* (Barlow et al. 2013). More recently, Schilke et al. (2014) reported on their early detections of the ArH^+ $J = 1{-}0$ transition in absorption toward six bright continuum sources using *Herschel*-HIFI. The absorption patterns were unique in their appearances; ArH^+ showed up in all velocity components associated with diffuse foreground molecular clouds, but was conspicuously absent at velocities related to the sources themselves. The observations were reproduced by models in which argonium is present only in the almost purely atomic diffuse ISM, with peak abundance at molecular fractions in the 10^{-4} to 10^{-3} range. Basically, high values of ζ favor its formation, consistent with analyses of OH^+ and H_2O^+, which trace slightly higher, but still low H_2 fractions (see, e.g., Hollenbach et al. 2012; Indriolo et al. 2015), whereas molecular fractions $\gtrsim 10^{-3}$ favor its destruction by the reaction with H_2 to produce Ar and H_3^+. Although ArH^+ abhors molecular clouds, it does rely upon a small amount of

⋆ Appendix A is available in electronic form at http://www.aanda.org

H_2 for its existence. Moreover, with its specificity to the ISM with a molecular fraction of $\lesssim 10^{-3}$, it is a much better tracer of the almost purely atomic ISM than the 21 cm hyperfine structure line of atomic hydrogen, because the latter is also seen in the ISM with a molecular fraction of 0.01 or even larger than 0.5 (Schilke et al. 2014). Argonium may also be used to infer ζ in combination with other tracers.

Because argonium is ubiquitous in the Galactic diffuse ISM, the next step is to search for it in extragalactic sources. The $J = 1-0$ transition of $^{36}ArH^+$ at 617525.23 ± 0.15 MHz[1] is close to a strong atmospheric water line ($5_{32}-4_{41}$ near 620.7 GHz)[2], and the $^{38}ArH^+$ transition is less than 900 MHz lower in frequency. Therefore, ground-based observations of ArH^+ in absorption in nearby galaxies are very difficult. As *Herschel* is no longer in operation and SOFIA has no receiver at these frequencies yet, searches toward galaxies at low to moderate redshifts are more promising, given the current instrumental capabilities.

The unnamed foreground galaxy at $z = 0.88582$ (Wiklind & Combes 1996) in the direction of the blazar PKS 1830−211 is particularly well suited for such searches. The galaxy is lensing the background radiation coming from the blazar (Pramesh Rao & Subrahmanyan 1988; Subrahmanyan et al. 1990); two images, to the SW and NE of the blazar and separated by 1″, are especially strong. Absorption spectra toward the SW and NE images probe two separate lines of sight across this foreground galaxy located on opposite sides of the nucleus. For most species, the absorption toward the SW image is much stronger than that toward the NE image, since it probes denser gas, with higher H_2 column densities. The blazar itself appears to be devoid of line-absorption or emission at radio frequencies. The line of sight toward the SW image of PKS 1830-211 is, to date, the extragalactic object with the largest number of molecules detected (~40, see Muller et al. 2011, 2014b).

The redshift $z = 0.89$ corresponds to a look-back time of ~7.5 Gyr, when the Universe was slightly less than half its current age. At that time, the enrichment of the ISM with heavy elements was dominated by massive stars. This could lead to isotopic ratios of the elements different from those in the local galactic ISM. Molecular species may be much more promising in this regard than atoms, because of their more distinct spectroscopic patterns, e.g. different rotational patterns, caused by differences in the reduced masses. Indeed, isotopic ratios have been determined in the foreground galaxy for molecules containing moderately heavy elements such as Si, S, and Cl in addition to C, N, and O, and show some differences compared to their solar values (Muller et al. 2006, 2011, 2014a).

The Atacama Large Millimeter/submillimeter Array (ALMA) now offers high sensitivity and wide frequency coverage for spectroscopic studies. Already in the Early Science Cycle 0, despite the limited number of antennas and only four spectral tunings, a large number (17) of common interstellar species, such as CO, CH, H_2O, HCO^+, HCN, C_2H, and NH_3, were observed toward PKS 1830−211, including two new extragalactic detections, H_2Cl^+ (Muller et al. 2014a) and NH_2 (see Muller et al. 2014b, for the presentation of the ALMA Cycle 0 survey and overall results).

The present Letter reports the first extragalactic detection of $^{36}ArH^+$ and $^{38}ArH^+$ from ALMA observations toward PKS 1830−211.

[1] From the CDMS catalog (Müller et al. 2001, 2005), see also Sect. 2.
[2] See, e.g., the JPL catalog (Pickett et al. 1998).

2. Observations and spectroscopic data

Observations reported here were obtained with ALMA on 2015 May 19 (Cycle 2), in about 20 min on-source time under very good atmospheric conditions (precipitable amount of water vapor of ~0.3 mm) and with receivers tuned to ~327 GHz (Band 7)[3]. The three ArH^+ isotopologs were observed simultaneously in the same 1.875 GHz wide spectral window. Two additional spectral windows were centered at ~337 GHz to cover the H_2O^+ $1_{10}-1_{01}$, $J = 0.5-1.5$ line (rest frequency 634.27 GHz) and at ~339 GHz (no lines were detected in this window, which was used to map the continuum). The bandpass response of the antennas was calibrated using the radio-bright quasar J1924−2914, and the gain solutions versus time were determined from observations of the quasar J1832−2039, within 1° on the sky from PKS 1830−211. The overall standard calibration was applied by the ALMA pipeline. One more step of self-calibration was performed and calibrated visibilities were then fit with the task UVMULTIFIT (Martí-Vidal et al. 2014) to extract the spectra toward the point-like SW and NE images of PKS 1830−211. The two images (separated by ~1″) were well resolved by the synthesized beam of ~0.5″. The velocity resolution is 1.0 km s^{-1} after Hanning smoothing. Two atmospheric lines due to O_3 (at 326.901 and 327.845 GHz)[2] show up in the spectra (Fig. 1). They are easily identified and disentangled from absorption intrinsic to the source, since they occur at the same frequency in both SW and NE spectra, see Fig. A.1.

Spectroscopic data of ArH^+ transitions were taken from the CDMS (Müller et al. 2001, 2005) and are summarized in Table 1. An isotopic invariant fit of diverse rotational and rovibrational data was carried out, similar to Odashima et al. (1999), to determine spectroscopic parameters of the molecule and to derive rest frequencies of rotational transitions of argonium isotopologs. The most relevant data for our observations are the $J = 1-0$ transitions of $^{36}ArD^+$, $^{38}ArD^+$, and $^{40}ArD^+$ from Bowman et al. (1983). As ^{40}Ar is the most abundant Ar isotope on Earth, almost all of the remaining rotational (Liu et al. 1987; Brown et al. 1988; Odashima et al. 1999) and rovibrational data (Brault & Davis 1982; Johns 1984; Filgueira & Blom 1988) used in that calculation refer to $^{40}ArH^+$ or to $^{40}ArD^+$. The $^{40}ArH^+$ ground state dipole moment is 2.18 D (Cheng et al. 2007).

3. Results and discussion

3.1. Column densities and abundances

Absorption signatures due to $^{36}ArH^+$ and $^{38}ArH^+$ were detected with good to very good signal-to-noise ratios toward both images of PKS 1830−211, SW and NE, see Fig. 1. The images and overview spectra are shown in Fig. A.1 in the Appendix.

Toward the SW image, a simple fit with one Gaussian velocity component and the same width and velocity offset for both isotopologs yields a centroid velocity of 5.6 ± 0.4 km s^{-1} and a full width at half maximum of 57.3 ± 0.8 km s^{-1}, which, to first order, reproduces well both $^{36}ArH^+$ and $^{38}ArH^+$ absorptions. Integrated opacities of 13.64 ± 0.19 and 3.89 ± 0.16 km s^{-1} were derived for $^{36}ArH^+$ and $^{38}ArH^+$, respectively. We obtain only an upper limit of 0.42 km s^{-1} (at 3σ confidence level) in the case of $^{40}ArH^+$. However, the ArH^+ line profile shows a slight deviation from a simple Gaussian, and fit results and values of integrated opacity over velocity channels from −80 to +110 km s^{-1}

[3] At $z = 0.89$, the frequencies of the $J = 1-0$ line of ArH^+ isotopologs are redshifted close to the $5_{15}-4_{22}$ atmospheric water line near 325.2 GHz[2].

Table 1. Spectroscopic data[a] of the $J = 1-0$ transitions of ArH^+ isotopologs observed in the present study.

Species	Rest frequency (MHz)	A_{ij}[b] (10^{-3} s^{-1})	E_{low} (K)	$\int \tau dv$(SW)[c] (km s^{-1})	Δv(SW)[d] (km s^{-1})	v_{off}(SW)[e] (km s^{-1})	$\int \tau dv$(SW)[f] (km s^{-1})	$\int \tau dv$(NE)[g] (km s^{-1})
$^{36}ArH^+$	617 525.23 (15)	4.33	0.0	13.65 (17)	57.3 (8)	5.6 (4)	15.88 (21)	7.61 (12)
$^{38}ArH^+$	616 648.76 (8)	4.31	0.0	3.90 (15)	57.3 (8)	5.6 (4)	4.59 (21)	1.68 (12)
$^{40}ArH^+$	615 858.15 (5)	4.30	0.0				<0.42[h]	

Notes. [a] Numbers in parentheses are one standard deviation in units of the least significant figures. [b] Einstein A value. [c] Velocity integrated optical depth toward the SW image from a single Gaussian fit. [d] Full width at half maximum of main SW image feature from that fit constrained to be equal for all three species. [e] Offset of main SW image centroid velocity with respect to the systemic velocity from that fit constrained to be equal for all three species. [f] Optical depth toward the SW image integrated over channels from −80 to +110 km s^{-1}. [g] Optical depth toward the NE image integrated over channels from −280 to −80 km s^{-1}. [h] Upper limit, 3σ uncertainty.

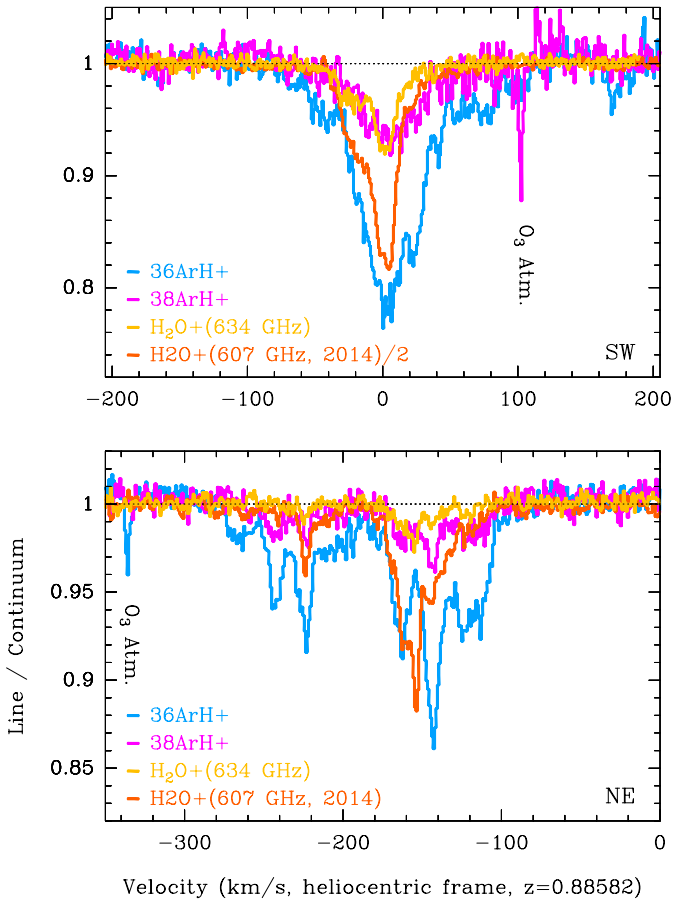

Fig. 1. Spectra of $^{36}ArH^+$ and $^{38}ArH^+$ toward PKS 1830−211 SW (*top*) and NE (*bottom*) images, together with two *para*-H_2O^+ fine structure lines of the $1_{10}-1_{01}$ transition; none of the transitions shows hyperfine splitting.

are given in a separate column in Table 1. The weak velocity component at +170 km s^{-1}, previously only detected in the lines of HCO^+, HCN, and H_2O and all three strongly saturated near $v = 0$ km s^{-1} (Muller et al. 2011, 2014b), is − surprisingly − also detected in the $^{36}ArH^+$ spectrum.

In contrast to the SW line of sight, where the absorption mostly resides in one bulky absorption feature (with the exception of the additional +170 km s^{-1} component), the ArH^+ absorption profile toward the NE image shows a remarkable series of narrow (a few km s^{-1}) features spanning over ∼200 km s^{-1}, also seen, e.g., in the absorption profile of H_2O (Muller et al. 2014b).

With the assumptions that the rotational excitation temperature is equal to the radiation temperature of the cosmic microwave background at $z = 0.89$, 5.14 K, and that the lines are optically thin, the total column densities of $^{36}ArH^+$ along the SW and NE lines of sight are 2.7×10^{13} cm^{-2} and 1.3×10^{13} cm^{-2}, respectively, i.e., differing by only a factor ∼2. Muller et al. (2014a) found a similar ratio of ∼3 for H_2Cl^+. In contrast, the H_2 column density, estimated from proxies such as CH, is about one order of magnitude higher toward SW (Muller et al. 2014b). The NE line of sight is known to be more diffuse and richer in atomic gas (Koopmans & de Bruyn 2005), thus the enhancement of ArH^+ on the NE line of sight relative to the SW one is not surprising. The detection of the ArH^+ absorption in the +170 km s^{-1} velocity component toward the SW image suggests that this region has a low molecular fraction as well, or that time variations (Muller & Guélin 2008) have made this feature stronger.

Since it is expected that ArH^+ traces a gas component with a very low H_2/H fraction, it would seem natural to compare its absorption profile with that of H I. The H I absorption has been previously observed toward the blazar[4] (Chengalur et al. 1999; Koopmans & de Bruyn 2005), but only at low angular resolution, not resolving the background continuum morphology. PKS 1830−211 is radically different at centimeter and submm wavelengths: the NE and SW images, which are point-like in the submm, are more extended in the cm; in addition, the emission from the pseudo Einstein ring can be seen in the cm regime (Subrahmanyan et al. 1990). Thus, comparison of spectra between such different frequencies is not straightforward.

Both H_2O^+ and ArH^+ trace the diffuse ISM component (Indriolo et al. 2015). Therefore, one may assume that both species show similar absorption features. This is not the case toward either of the PKS 1830−211 images, as can be seen in Fig. 1; this also demonstrated in a correlation plot (Fig. A.2) in the Appendix. The 634 GHz line of H_2O^+ was observed simultaneously with ArH^+, while the 607 GHz line, with a higher relative intensity and better signal-to-noise ratio, was observed in 2014 (Muller et al., in prep.). There appear to be no large variations in the H_2O^+ spectra, which were observed about one year apart. A poor correlation between the two molecular ions is also seen in Galactic sources (Schilke et al. 2014), suggesting that the diffuse ISM with a molecular fraction 10^{-4} to 10^{-3} (as traced by ArH^+) is different from the diffuse ISM with a molecular fraction around 0.04 (as traced by H_2O^+). It is conceivable that at least part of ArH^+ absorption arises in the warm (8000 K) ionized medium (WIM), rather than entirely in the least molecular

[4] See also http://www.atnf.csiro.au/projects/askap/news_commissioning_10042014.jpg

parts of the diffuse, neutral ISM. A detailed discussion of the chemistry of the WIM will be presented elsewhere.

3.2. The $^{36}Ar/^{38}Ar$ isotopic ratio at z = 0.89

The $^{36}Ar/^{38}Ar$ ratio is 3.46±0.16 (integrated over velocities from −80 to +110 km s^{-1}; 3.50 ± 0.14 from the Gaussian fit) toward the SW image, significantly lower than the solar value 5.50 ± 0.01 (Vogel et al. 2011), or the terrestrial value of 5.305 ± 0.068 (Berglund & Wieser 2011). Although ^{40}Ar (from the radio-active decay of ^{40}K) is dominant on Earth, we note that it plays only a minor role in the ISM. The α elements sulfur and silicon also show ratios about two times lower than their terrestrial values (see Muller et al. 2006, 2011). In contrast, the $^{35}Cl/^{37}Cl$ ratio was found to be identical to the terrestrial value (Muller et al. 2014a). The $^{36}Ar/^{38}Ar$ ratio toward the NE image is 4.53 ± 0.33, between the SW ratio and the solar and terrestrial values and compatible with either within the uncertainties. The 3σ limit for the $^{38}ArH^+/^{40}ArH^+$ ratio of >11 is not constraining considering the solar ratio of ~615 (Vogel et al. 2011), which is assumed to be close to the value in the local ISM.

Kobayashi et al. (2006) calculated nucleosynthesis yields of core-collapse supernovae (SNe) and hypernovae (HNe, which are more energetic by an order of magnitude) to predict the evolution of isotopic ratios in the Milky Way, SNe and HNe being the dominant contributors to elements from Na to Fe with the possible exception of a few selected isotopes. They presented yields for different progenitor masses and metallicities, and subsequently incorporated the results into models for the enrichment of the Milky Way (Kobayashi et al. 2011). While the nucleosynthetic yields for many elements, including ^{36}Ar and ^{38}Ar, show a non-monotonic dependence on progenitor mass, the predicted $^{36}Ar/^{38}Ar$ ratio tends to decline with increasing metallicity and is typically smaller for HNe than for SNe. Nevertheless, even for the highest metallicities considered in the Milky Way enrichment models (Z = 0.02, or solar metallicity), the predicted $^{36}Ar/^{38}Ar$ ratio is larger than the observed ratio in either the Sun or the PKS 1830−211 absorber. There are several uncertain assumptions in the nucleosynthesis and Galactic enrichment models, including the importance of convective mixing in the progenitor stars and the relative frequency of HNe; observations of isotopic ratios in diverse environments, such as those presented here, promise to provide valuable constraints for future models. There is no evidence for low metallicity in the foreground galaxy, but the exact value cannot be determined at present.

4. Conclusion

We have detected for the first time extragalactic argonium in both of its important interstellar isotopologs. Therefore, ArH^+ is not only a good tracer of the almost purely atomic diffuse ISM in the Milky Way, but it is also suitable for investigations of extragalactic sources, possibly to a similar extent as OH^+ or H_2O^+. It will be interesting to search for ArH^+ in a selection of galaxies at moderately low to higher redshifts to obtain a more complete picture of the atomic component of the extragalactic ISM and to look for possible trends in the $^{36}Ar/^{38}Ar$ ratio with redshift. The Si, S, Cl, and Ar isotopic ratios appear to be promising probes into the nucleosynthesis in the early Universe because their yield ratios depend strongly on the type of supernova, and all four elements form molecules that have been detected even in distant galaxies. It will be interesting to see if these ratios correlate with ζ as both aspects are affected by SN activity. Searches for argonium in nearby galaxies may be more promising with the potential future GREAT receiver on board SOFIA. Combined observations of ArH^+ with OH^+, H_2O^+, and HF or CH will provide insight into the partitioning of atomic and molecular hydrogen and into the cosmic ray ionization rate. Such an analysis is currently under way for PKS 1830−211 and will be published separately.

Acknowledgements. This paper makes use of the following ALMA data: ADS/JAO.ALMA#2013.1.00296.S. ALMA is a partnership of ESO (representing its member states), NSF (USA) and NINS (Japan), together with NRC (Canada) and NSC and ASIAA (Taiwan) and KASI (Republic of Korea), in cooperation with the Republic of Chile. The Joint ALMA Observatory is operated by ESO, AUI/NRAO and NAOJ. The present investigations have been supported by the Deutsche Forschungsgemeinschaft (DFG) in the framework of the collaborative research grant SFB 956, projects A4 and C3. Support for this work was also provided by NASA through an award issued by JPL/Caltech. Our research benefited from NASA's Astrophysics Data System (ADS).

References

Barlow, M. J., Swinyard, B. M., Owen, P. J., et al. 2013, Science, 342, 1343
Berglund, M., & Wieser, M. E. 2011, Pure Appl. Chem., 83, 397
Bowman, W. C., Plummer, G. M., Herbst, E., & de Lucia, F. C. 1983, J. Chem. Phys., 79, 2093
Brault, J. W., & Davis, S. P. 1982, Phys. Scr., 25, 268
Brown, J. M., Jennings, D. A., Vanek, M., Zink, L. R., & Evenson, K. M. 1988, J. Mol. Spectr., 128, 587
Cheng, M., Brown, J. M., Rosmus, P., et al. 2007, Phys. Rev. A, 75, 012502
Chengalur, J. N., de Bruyn, A. G., & Narasimha, D. 1999, A&A, 343, L79
De Luca, M., Gupta, H., Neufeld, D., et al. 2012, ApJ, 751, L37
Filgueira, R. R., & Blom, C. E. 1988, J. Mol. Spectr., 127, 279
González-Alfonso, E., Fischer, J., Bruderer, S., et al. 2013, A&A, 550, A25
Hollenbach, D., Kaufman, M. J., Neufeld, D., et al. 2012, ApJ, 754, 105
Indriolo, N., Neufeld, D. A., Gerin, M., et al. 2015, ApJ, 800, 40
Johns, J. W. C. 1984, J. Mol. Spectr., 106, 124
Kobayashi, C., Umeda, H., Nomoto, K., Tominaga, N., & Ohkubo, T. 2006, ApJ, 653, 1145
Kobayashi, C., Karakas, A. I., & Umeda, H. 2011, MNRAS, 414, 3231
Koopmans, L. V. E., & de Bruyn, A. G. 2005, MNRAS, 360, L6
Lis, D. C., Pearson, J. C., Neufeld, D. A., et al. 2010, A&A, 521, L9
Liu, D.-J., Ho, W.-C., & Oka, T. 1987, J. Chem. Phys., 87, 2442
Martí-Vidal, I., Vlemmings, W., Muller, S., & Casey S. 2014, A&A, 563, A136
Menten, K. M., Wyrowski, F., Belloche, A., et al. 2011, A&A, 525, A77
Muller, S., & Guélin, M. 2008, A&A, 491, 739
Muller, S., Guélin, M., Dumke, M., Lucas, R., & Combes, F. 2006, A&A, 458, 417
Muller, S., Beelen, A., Guélin, M., et al. 2011, A&A, 535, A103
Muller, S., Black, J. H., Guélin, M., et al. 2014a, A&A, 566, L6
Muller, S., Combes, F., Guélin, M., et al. 2014b, A&A, 566, A112
Müller, H. S. P., Thorwirth, S., Roth, D. A., & Winnewisser, G. 2001, A&A, 370, L49
Müller, H. S. P., Schlöder, F., Stutzki, J., & Winnewisser, G. 2005, J. Mol. Struct., 742, 215
Neufeld, D. A., Falgarone, E., Gerin, M., et al. 2012, A&A, 542, L6
Odashima, H., Kozato, A., Matsushima, F., Tsunekawa, S., & Takagi, K. 1999, J. Mol. Spectr., 195, 356
Ossenkopf, V., Müller, H. S. P., Lis, D. C., et al. 2010, A&A, 518, L111
Pickett, H. M., Poynter, R. L., Cohen, E. A., et al. 1998, J. Quant. Spectr. Rad. Transf., 60, 883
Pramesh Rao, A., & Subrahmanyan, R. 1988, MNRAS, 231, 229
Schilke, P., Lis, D. C., Bergin, E. A., Higgins, R., & Comito, C. 2013, J. Phys. Chem. A, 117, 9766
Schilke, P., Neufeld, D. A., Müller, H. S. P., et al. 2014, A&A, 566, A29
Subrahmanyan, R., Narasimha, D., Pramesh Rao, A., & Swarup, G. 1990, MNRAS, 246, 263
van der Werf, P. P., Isaak, K. G., Meijerink, R., et al. 2010, A&A, 518, L42
Vogel, N., Heber, V. S., Baur, H., Burnett, D. S., & Wieler, R. 2011, Geochim. Cosmochim. Acta, 75, 3057
Weiß, A., Requena-Torres, M. A., Güsten, R., et al. 2010, A&A, 521, L1
Wiklind, T., & Combes, F. 1996, Nature, 379, 139
Wyrowski, F., Menten, K. M., Güsten, R., & Belloche, A. 2010, A&A, 518, A26

Appendix A: Complementary figures

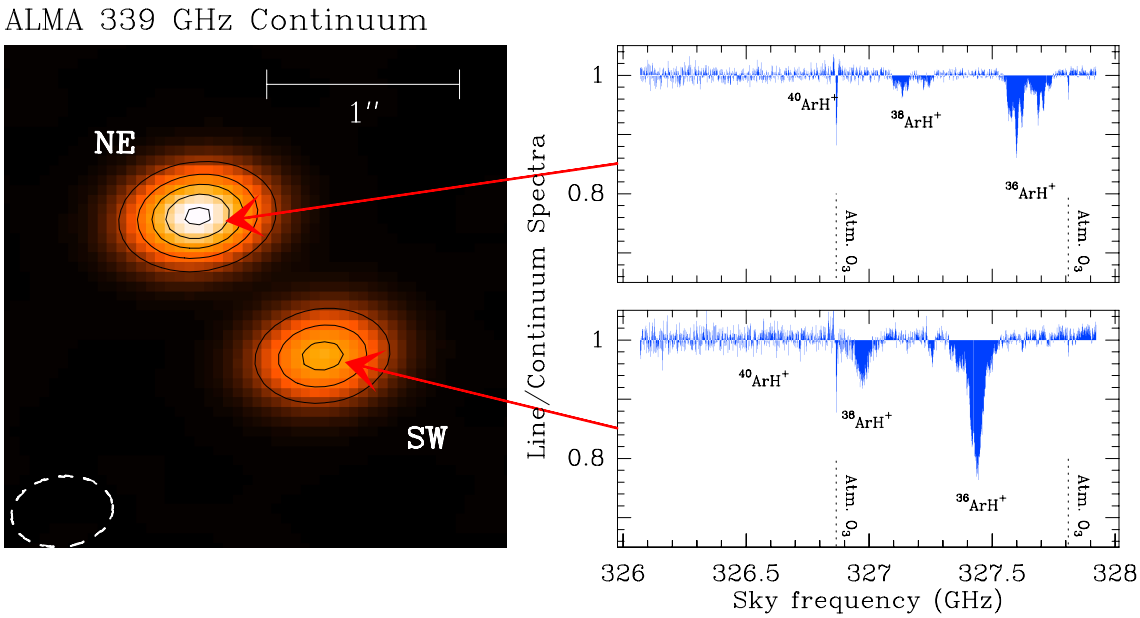

Fig. A.1. Map of the 339 GHz continuum emission of PKS 1830−211 showing the two resolved lensed images of the blazar (*left*). Overview of the ArH^+ absorption spectrum toward PKS 1830−211 SW (*bottom right*) and NE (*top right*) from the current observations. Expected positions of the main absorption feature are indicated for $^{36}ArH^+$, $^{38}ArH^+$, and $^{40}ArH^+$; the last is not detected. The noise increases toward lower frequencies because of the proximity of the atmospheric water line near 325.2 GHz.

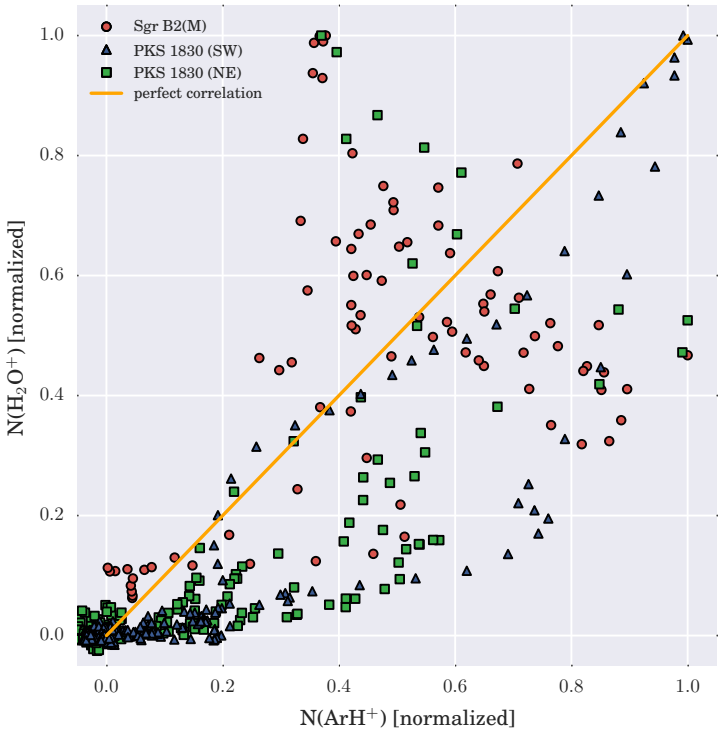

Fig. A.2. Normalized correlation plot of H_2O^+ versus $^{36}ArH^+$ toward PKS 1830−211 SW, NE, and Sagittarius B2(M). The column densities of the two species have been normalized by the maximum values for each component and for each velocity channel. A perfect correlation (i.e. just a constant scaling factor between the two species) would result in clustering along the yellow line. The distributions of the two cations are poorly correlated toward the sources. The PKS 1830−211 data are from this work and from Muller et al. (in prep.) for $^{36}ArH^+$ and H_2O^+, respectively; the corresponding Sagittarius B2(M) data are from Schilke et al. (2014) and Schilke et al. (2013).